Deep-Ultraviolet Micro-LEDs Exhibiting High Output Power and High Modulation Bandwidth Simultaneously

Duo Li, Shangfeng Liu, Zeyuan Qian, Quanfeng Liu, Kang Zhou, Dandan Liu, Shanshan Sheng, Bowen Sheng, Fang Liu, Zhaoying Chen, Ping Wang, Tao Wang, Xin Rong, Renchun Tao, Jianbin Kang, Feiliang Chen, Junjie Kang, Ye Yuan, Qi Wang, Ming Sun, Weikun Ge, Bo Shen, Pengfei Tian, and Xinqiang Wang*

Deep-ultraviolet (DUV) solar-blind communication (SBC) shows distinct advantages of non-line-of-sight propagation and background noise negligibility over conventional visible-light communication. AlGaN-based DUV micro-light-emitting diodes (μ-LEDs) are an excellent candidate for a DUV-SBC light source due to their small size, low power consumption, and high modulation bandwidth. A long-haul DUV-SBC system requires the light source exhibiting high output power, high modulation bandwidth, and high rate, simultaneously. Such a device is rarely reported. A parallel-arrayed planar (PAP) approach is here proposed to satisfy those requirements. By reducing the dimensions of the active emission mesa to micrometer scale, DUV μ-LEDs with ultrahigh power density are created due to their homogeneous injection current and enhanced planar isotropic light emission. Interconnected PAP μ-LEDs with a diameter of 25 μm are produced. This device has an output power of 83.5 mW with a density of 405 W cm^{-2} at 230 mA, a wall-plug efficiency (WPE) of 4.7% at 155 mA, and a high −3 dB modulation bandwidth of 380 MHz. The remarkable high output power and efficiency make those devices a reliable platform to develop high-modulation-bandwidth wireless communication and to meet the requirements for bio-elimination.

1. Introduction

Group III nitride materials and devices have experienced rapid development over the past two decades.[1] In virtue of its direct and wide bandgap, high-efficiency light-emitting diodes (LEDs) ranging from the infrared to ultraviolet bands have been realized.[1a] Since the first report on ultraviolet (UV) LEDs with an emission wavelength shorter than 360 nm in 1998,[1b] a new era of AlGaN-based deep-UV (DUV) LEDs has been started.

Creating a solar-blind communication (SBC), which operates at a wavelength between 200 and 280 nm, has attracted significant interest. Compared to conventional visible-light communication, using DUV wavelength (200–280 nm) light as a signal carrier for SBC has unique features such as background noise negligibility,[1c] non-line-of-sight communication, and so

D. Li, S. Liu, S. Sheng, B. Sheng, F. Liu, Z. Chen, P. Wang, X. Rong, R. Tao, W. Ge, B. Shen, X. Q. Wang
State Key Laboratory for Mesoscopic Physics and Frontiers Science Center for Nano-Optoelectronics
School of Physics
Peking University
Beijing 100871, China
E-mail: wangshi@pku.edu.cn

Z. Qian, P. Tian
School of Information Science and Technology
Fudan University
Shanghai 200438, China

Q. Liu, K. Zhou, D. Liu, M. Sun
Dongguan Sino Crystal Semiconductor Co., Ltd.
Dongguan 523500, China

T. Wang
Electron Microscopy Laboratory
School of Physics
Peking University
Beijing 100871, China

J. Kang
Microsystem and Terahertz Research Center
China Academy of Engineering Physics
Chengdu 610200, China

F. Chen
School of Electronic Science and Engineering
University of Electronic Science and Technology of China
Chengdu 611731, China

J. Kang, Y. Yuan
Songshan Lake Materials Laboratory
Dongguan 523808, China

Q. Wang, X. Q. Wang
Dongguan Institute of Opto-Electronics Peking University
Dongguan 523808, China

B. Shen, X. Q. Wang
Collaborative Innovation Center of Quantum Matter
School of Physics
Peking University
Beijing 100871, China

X. Q. Wang
Peking University Yangtze Delta Institute of Optoelectronics
Nantong, Jiangsu 226010, China

on.[2] It provides high security for military-tactical communication systems.[3] Its advantages include better pointing, acquisition, and tracking accuracy.[4] Even though traditional DUV light sources, i.e., mercury lamps, can be used in the SBC system,[6] their high power consumption, large volume, and low modulation bandwidth hinder their further development. On the contrary, AlGaN-based LEDs [5] exhibit potentials for their wavelength tunability, compact size, and long lifetime. Especially, with the rising international awareness of environmental protection, the replacement for mercury lamps by AlGaN-based DUV LEDs has been progressively put on the agenda after the International Minamata Convention in 2013.

For SBC application, AlGaN-based DUV micro-LEDs (μ-LEDs),[5e,5f] with the emission region (mesa) dimension down to sub-100 μm range, are the best candidate for their improved modulation bandwidth in virtue of the small resistance–capacitance (RC) time constant,[7] high current densities, and short carrier lifetime.[1c] At present time, DUV μ-LEDs, working around 270 nm, have achieved a 400 MHz modulation bandwidth.[1c] However, its light output power (LOP) is relatively small with a value of <1 mW and wall-plug efficiency (WPE) is smaller than 1%. These values are too low to satisfy the requirement of a long transmission distance. Therefore, to promote the prospect of III-nitride materials in SBC application, it is necessary to improve the performances of AlGaN-based DUV LEDs. Besides, such an improvement can surely benefit other application fields with III-nitrides, for example, sterilization and water purification. Unfortunately, it is difficult to improve either WPE or LOP, and even more difficult to improve both simultaneously.

Better light extraction and homogeneous current spreading are two aspects to improve those essential requirements. The main topics for improving the amount of light are extracting the transverse-magnetic (TM) polarized light,[9] reducing the light loss from the absorption in the p-GaN layer, and overcoming light internal reflections at layer interfaces.[10] Transparent p-type electrodes,[11] highly reflective mirrors on the top and sidewall of the mesa region,[12] and micro/nanocontacts[13] have been proposed to decrease the light absorption loss. The substrate surface texturing method[14] and patterning the sapphire substrate[15] have further reduced the light internal reflection. In the case of current spreading, the low conductivity of Al-rich AlGaN can degrade the internal quantum efficiency of the DUV LEDs.[16] Optimizing the conductivity of the n-AlGaN,[17] inserting a dielectric layer under the p-electrode,[18] and modifying the p-electrode patterns[19] have been tried to solve the current crowding problem. There has been some progress in improving the performance of large-chip-sized DUV LEDs, but these issues become more critical when the emission region is reduced. Till date, the performance of DUV LEDs is far less than expected. There is still ample room to improve.

Here, we propose a parallel-arrayed planar (PAP) μ-LED strategy to improve the LOP and WPE. The improvements with PAP μ-LED strategy have the following aspects: 1) the light absorption from the p-type Ohmic contact layer, which is generally selected as nickel, is reduced by using microcontacts on top of the p-GaN.[20] 2) The cylinder-shaped mesa is coated with a reflective Al mirror to achieve isotropic light extraction, which is independent of the emission angle.[21] 3) A homogeneous

current distribution can be achieved. By doing that, the current crowding effect, which has been an open challenge in the large-chip-sized LEDs,[16] is solved. 4) The current density can be increased to higher than 1000 A cm^{-2} by reducing the size of the emission region to 25 μm. This achievement satisfies the requirement for high modulation bandwidth communication. 5) The mesa with a smaller size shows a less discrepancy of tensile stress distribution in the emission region. This is beneficial for decreasing the proportion of the TM-polarized emission according to theoretical calculations and experiments in previous reports.[22] Using these improvements, a PAP μ-LED chip with a 25 μm mesa is achieved showing a maximum light output power of 83.5 mW and a maximum WPE of 4.7%. These values are much higher than most commercial devices. More importantly, the PAP μ-LEDs reached a −3 dB modulation bandwidth of 380 MHz at the same time, which is available for SBC application. This work provides a path for advancing the application of DUV LEDs for sterilization-co-communication.

2. Results and Discussions

Figure 1a,b shows schematic diagrams of flip-chip PAP μ-LEDs from cross-sectional and plan views, respectively. The PAP μ-LEDs consist of an arrayed mesa whose cross-sectional structure is shown in Figure 1a, where the x-axis shows the direction vertical to the epitaxy structure of the DUV LED. The mesa region was fabricated via the plasma etching process to form a cylinder shape, which includes a p-GaN, p-AlGaN layer, an electron-blocking layer (EBL), multiple quantum wells (MQWs), and n-AlGaN layer. The Ni/Au and Ti/Al/Ti/Au were deposited as p-type and n-type Ohmic contact electrodes, respectively. A SiO$_2$ passivation layer isolates the p-type and n-type electrodes. An Al mirror was coated to enclose the side and top of those mesas to reflect DUV light and to connect the package pads with Ohmic contact electrodes as well. The devices whose mesas have diameters of 25, 50, 100, and 200 μm are named as PAP-0101, PAP-0202, PAP-0404, and PAP-0808, respectively. To ensure that each type of PAP μ-LEDs has the same total emission area (0.125 mm^2), PAP-0101, PAP-0202, PAP-0404, and PAP-0808 were designed to have 16×16, 8×8, 4×4, and 2×2 mesas, respectively. These designs are shown in Figure 1b in a plan view, where the arrayed green circles indicate the structure shown in Figure 1a. More details of these devices can be seen in Figure S1 (Supporting Information).

A Monte Carlo ray-tracing simulation has been performed as an initial approach to investigate the LOP of PAP μ-LEDs. Seven types of PAP devices were assumed to have 32×32, 16×16, 8×8, 4×4, 2×2, 1×1, and 1×1 mesas, and the diameters of these mesas were set to be 12.5, 25, 50, 100, 200, 300, and 400 μm, respectively. Moreover, uniformly distributed point light sources were assumed within the MQW layers, with each one having the same initial emission power and a 1:1 transverse-electric (TE)/TM ratio.[21] Please note that the extra nonradiative recombination centers induced by plasma etching on the sidewall were not considered in the simulation. Figure 1c shows that the simulated normalized LOP increases with decreasing mesa diameter and the value of LOP increases about eight times when the diameter was reduced from 400 to 12.5 μm. It
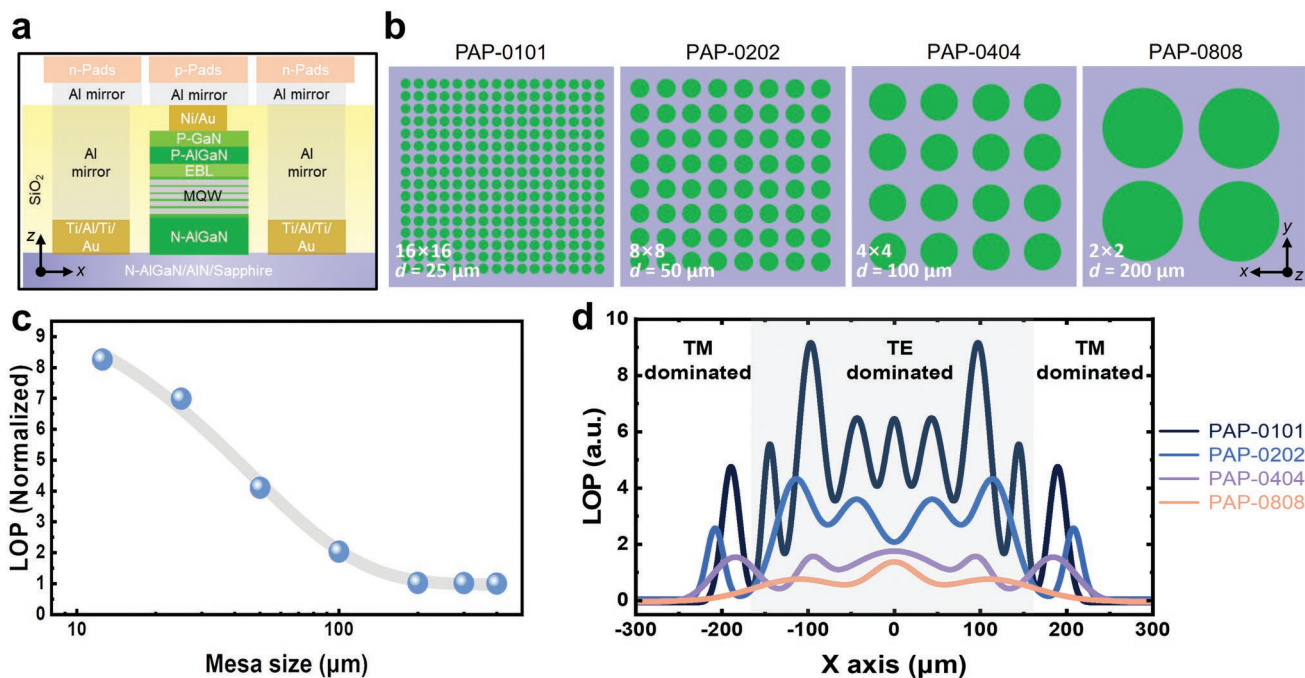
Figure 1. a) Schematic diagram of mesa region in cross-sectional view. b) Plan view diagrams of PAP-0101, PAP-0202, PAP-0404, and PAP-0808. c) Simulated normalized LOP varies as a function of the mesa diameter. d) Simulated LOP distribution of PAP-0101, PAP-0202, PAP-0404, and PAP-0808.

is, however, challenging to fabricate stable PAP μ-LEDs with a mesa diameter of 12.5 μm, fortunately, whose LOP is only 18% higher than the one with a diameter of 25 μm. For mesas with larger diameters (>200 μm), the LOP almost remains constantly low. Therefore, we only studied the LOP distribution of devices with mesa diameters of 25, 50, 100, and 200 μm, which are labeled as PAP-0101, PAP-0202, PAP-0404, and PAP-0808, as shown in Figure 1d. The detector is placed at the backside of the sapphire substrate to simulate the light collector of flip-chip DUV LEDs. The geometric dimensions of simulated devices including PAP-0101, PAP-0202, PAP-0404, and PAP-0808 are corresponding with those structures shown in Figure 1b. The backside of all devices is faced with the detector, which has a length of 340 μm. Therefore, the light collected from the backside in the range of 340 μm is considered as TE-dominated mode, with lights from other regions treated as TM-dominated mode. There are two significant features that can be observed from the simulated LOP distribution results when reducing the mesa size. One is that the intensity of both TE- and TM-polarized light is enhanced. The other is that more peaks appear with the number of interconnected mesas increasing, which indicates more light emitting from different azimuths.[21]

The LOP can be enhanced by using the PAP strategy due to the following reasons: 1) The area reduction of the p-GaN layer and the Ni/Au electrode decreases the light absorption loss. 2) The microscale mesa exposes much more sidewall area to emit photons. The Al mirror can thus reflect these photons which are emitted from the top and side of the mesa. 3) A parallel-arrayed design provides gaps between neighboring mesas without p-GaN and p-type electrodes. This can effectively reduce the light absorption loss because the light reflected from the layer interfaces (mainly AlN/sapphire and sapphire/air) can

pass through the gap and get reflected by the Al mirror, contributing to the final light output. Thus, the LOP can be reinforced by increasing the number of interconnected mesas with smaller sizes.

Besides, the nonuniform current distribution severely degrades the device performance, due to the poor conductivity of the Al-rich AlGaN, which brings about the current crowding effect.[23] We have theoretically calculated the current density distribution by a finite element method based on Shockley diode equations.[24] **Figure 2**a shows the equivalent model of PAP μ-LEDs with interconnected mesas sharing the same n-type electrode, which is used to compare the current distribution of PAP-0101, PAP-0202, PAP-0404, and PAP-0808 and to estimate the current density in different regions of the LED structure. The dashed lines with arrows marked as L1, L2, and L3, respectively, shown in Figure 2a indicate the detectors placed for calculating the current density. L1, L2, and L3 go across the in plane of the mesa region, the vertical and horizontal planes of remained n-AlGaN layer after etching, respectively. The calculated current density distributed in these detectors is plotted in Figure 2b–d. It is shown in Figure 2b that the PAP-0101 has the peak current density increasing about nine times higher than PAP-0808, due to the area reduction of the mesa and more carriers injected into the central region of the mesa.[25] Figure 2c shows that the current density of PAP-0101 is about six times in magnitude higher than PAP-0808. The larger transverse current flow indicates the lower voltage drop in the n-AlGaN layer. The current density of the n-AlGaN region beneath the n-type electrode of PAP-0101 is larger by a factor of 7 over PAP-0808 (Figure 2d). This enhancement indicates that the current crowding under the n-type electrodes becomes weaker. Figure 2e shows that PAP-0101 has the best
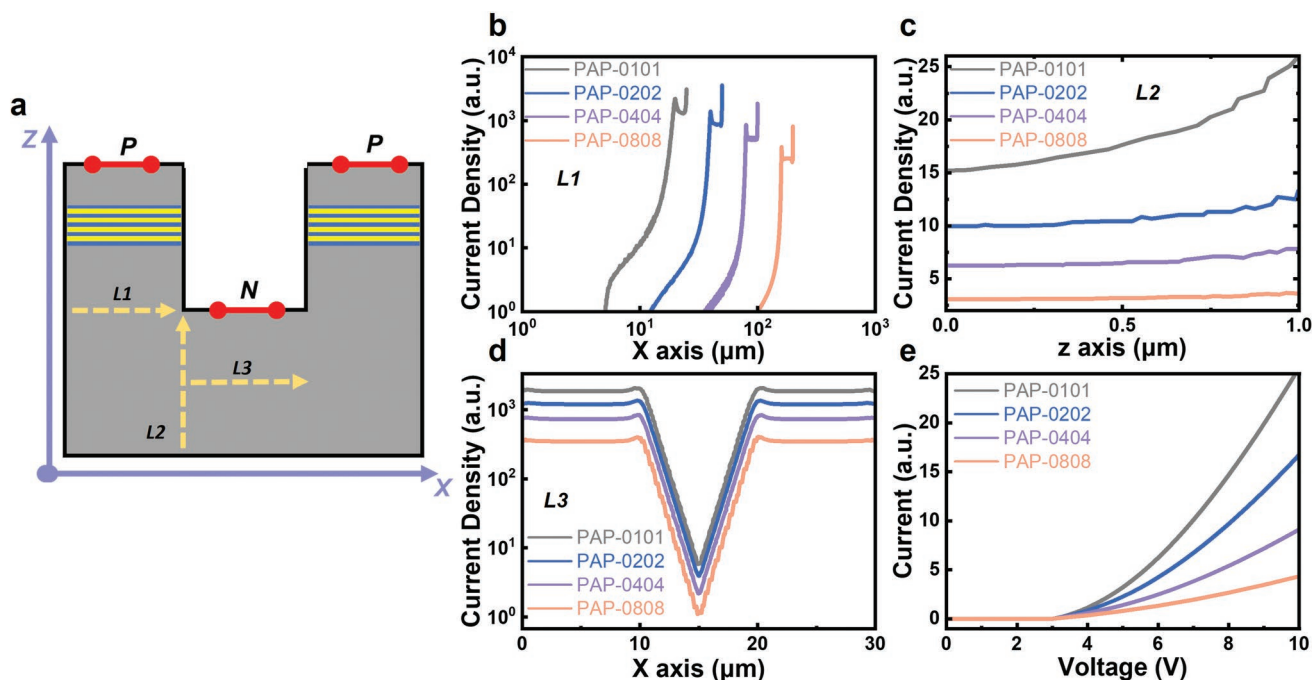
**ADVANCED
SCIENCE NEWS**

www.advancedsciencenews.com

**ADVANCED
MATERIALS**

www.advmat.de

Figure 2. a) A plot of the equivalent simulation model. The *z*-direction is parallel to the epitaxy direction. A detector is placed for calculating the current density, which is along the dashed line with an arrow of L1, L2, and L3, respectively. b–d) The calculated current densities and their distribution along the L1 (b), L2 (c), and L3 (d). e) Current–voltage (*I*–*V*) curves of PAP-0101, PAP-0202, PAP-0404, and PAP-0808.

electrical conductivity and the lowest forward voltage in all PAP devices due to the improvements of current density and uniformity as discussed before.

Following the simulation results, practical devices corresponding to PAP-0101, PAP-0202, PAP-0404, and PAP-0808 were fabricated with DUV LED wafers grown on nanopattern sapphire substrate by metal–organic chemical vapor deposition (MOCVD). **Figure 3**a,b shows the illustrative structure of the DUV LED wafer and high-angle annular dark-field scanning transmission electron microscopy (HAADF-STEM) image of the epitaxy, respectively. The epistructure includes n-type $Al_{0.64}Ga_{0.36}N$, five periods of $Al_{0.42}Ga_{0.58}N/Al_{0.5}Ga_{0.5}N$ quantum wells, $Al_{0.8}Ga_{0.2}N$ electron-blocking layer, p-type AlGaN, and p-type GaN.[26] These sharp interfaces indicate an excellent crystalline quality. Figure 3c shows the electroluminescence (EL) spectra of DUV LED wafer at different injected currents, where the strong emission is observed at the peak wavelength of 279 nm with a full width at half maximum of ≈12 nm. After obtaining the mesas by plasma etching, the wet etching process is used to remove the nonradiative sites induced by plasma bombardment (Figure S2, Supporting Information). Figure 3d shows the optical microscopy images of those PAP μ-LEDs, and each mesa is covered by the p-type electrode and surrounded by the n-type electrode. All PAP μ-LEDs have the same emission area as a conventional 1020 $(10 \times 20 \text{ mil}^2)$ device, which is typically made in a rectangle shape. The details of this device 1020 can be seen in Figure S3 (Supporting Information).

The LOP density (ρ_{out})[27] of DUV μ-LEDs was evaluated with an integrating sphere spectrum analyzer. As shown in **Figure 4**a, the LOP density decreases with the increasing mesa size, showing an inverse square relationship. It should be noted that a ρ_{out} of more than 400 W cm^{-2} was achieved when the mesa size was reduced to 25 μm. This significant enhancement of ρ_{out} indicates that many more holes and electrons can be injected into the active region for radiative recombination. Although the LOP of the standalone mesa with a small size is limited (the orange curve in Figure 4a),[28] this limitation can be overcome by PAP μ-LEDs' strategy. Figure 4b shows the relationship between LOP and applied current in the PAP μ-LEDs, where a conventional device 1020 with the same chip size as commercial products was fabricated from the same wafer to compare with PAP μ-LEDs. The LOP of device 1020 increases with an applied current, reaching a maximum LOP of ≈8 mW at 170 A cm^{-2} (120 mA), and then drops until breaking down at 210 A cm^{-2}. PAP-0202, PAP-0404, and PAP-0808 exhibit even lower LOP values of 2.2, 1.6, and 1.2 mW, respectively, although their maximum LOP appeared at large current density, which is higher than 700 A cm^{-2}. On the contrary, PAP-0101 exhibits a maximum LOP of ≈83.5 mW at 1150 A cm^{-2} (230 mA), almost an order higher than that of a conventional device 1020. Moreover, the LOP of PAP-0101 can keep over 50 mW in a wide current density range from 770 to 1440 A cm^{-2}. The WPE (i.e., LOP divided by electrical power consumption) was also evaluated for these devices and plotted in Figure 4c, where the PAP-0101 exhibits a maximum WPE of 4.7% at 775 A cm^{-2} (155 mA), about two times higher than a conventional device 1020 (2.5% at 7 A cm^{-2}). More importantly, the former was obtained at a current density 100 times higher than the latter, which is more important to applications such as long-haul communication and effective sterilization.

To further investigate the reason that causes the performance disparity in PAP devices with different mesa sizes, high-resolution micro-EL (μ-EL) measurements were performed to
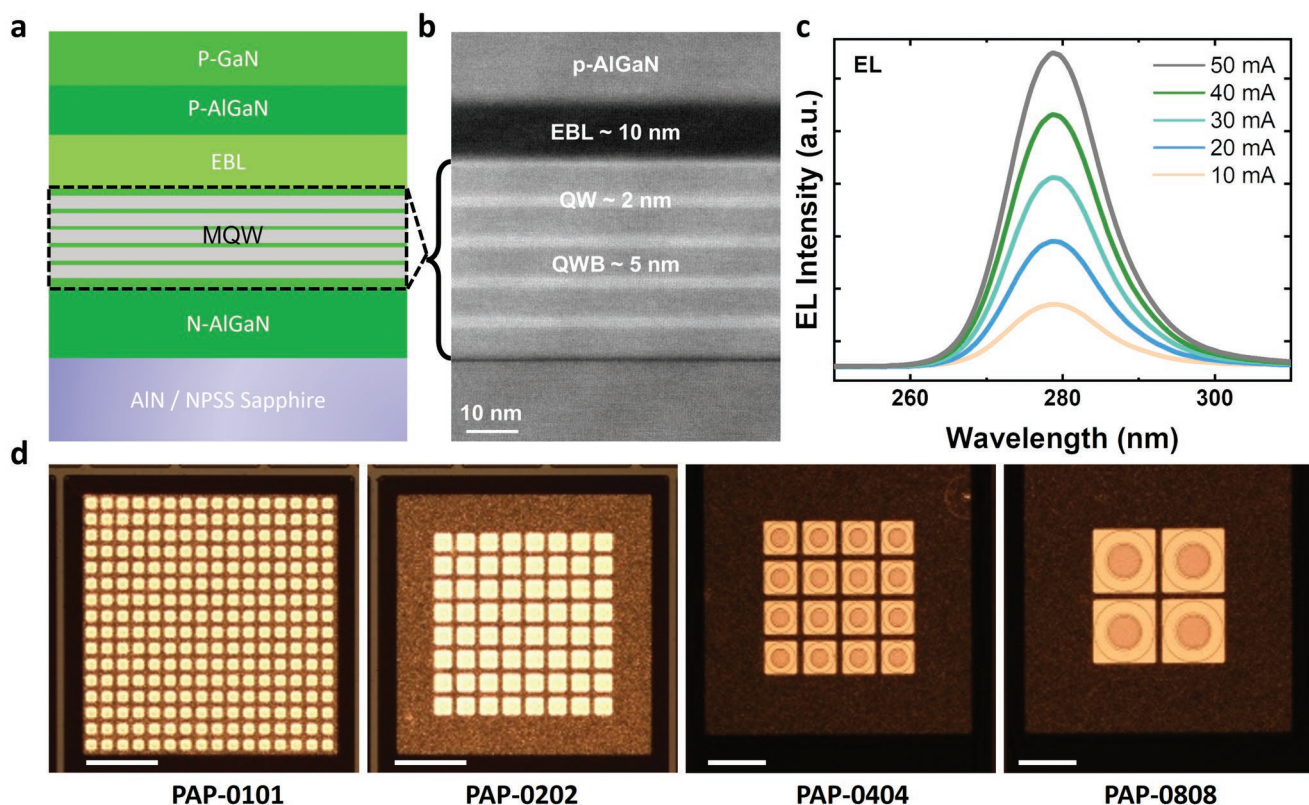
**ADVANCED
SCIENCE NEWS**

www.advancedsciencenews.com

**ADVANCED
MATERIALS**

www.advmat.de

Figure 3. a) Diagram of the epitaxy structure and b) cross-sectional HAADF-STEM of the DUV LEDs. c) EL spectra at various injection currents. The emission wavelength is 279 nm. d) Optical microscopy images of PAP-0101, PAP-0202, PAP-0404, and PAP-0808. The scale bar shown in each image is 200 µm.

investigate current spreading-dependent emission distribution. **Figure 5**a shows the optical microscopy images of a typical region for the succeeding µ-EL mapping acquisition of all PAP devices with a flip-chip package. All extracted EL spectra at the injected current of 150 mA are shown in Figure 5b. It is seen that the emission peak of PAP-0101 has a blueshift of about 1.3 nm in comparison to that of PAP-0808. This wavelength blueshift probably results from weakened quantum-confined Stark effect (QCSE) in the multiple quantum wells due the

relaxed compressive strain in the micro-LEDs with decreasing mesa size.[28b]

Figure 5c–f shows the EL mapping with intensity integrated from 279 to 281 nm. When a small current density is applied, both PAP-0101 and PAP-0202 show homogeneous emission covering the overall mesa (panels (i) and (ii) in Figure 5c,d), whereas the emission of PAP-0404 and PAP-0808 mainly comes from the edge region (panels (i) and (ii) in Figure 5e,f). With increasing currents (panels (iii) and (iv) in Figure 5c–f),
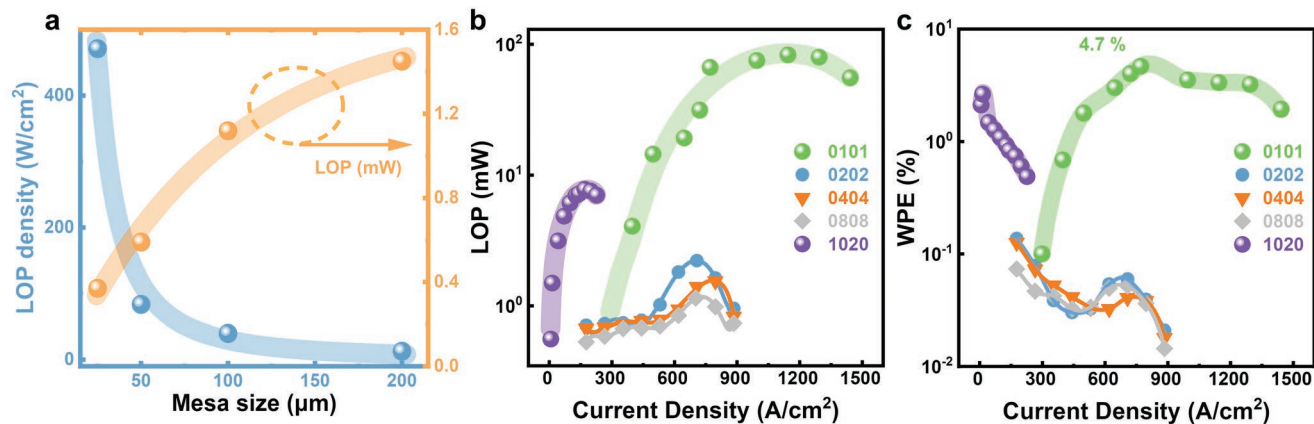

Figure 4. a) LOP and corresponding LOP density of the standalone-mesa device with various mesa sizes. b) Current-density-dependent LOP and c) wall-plug efficiency of PAP-0101, PAP-0202, PAP-0404, PAP-0808, and conventional device 1020.
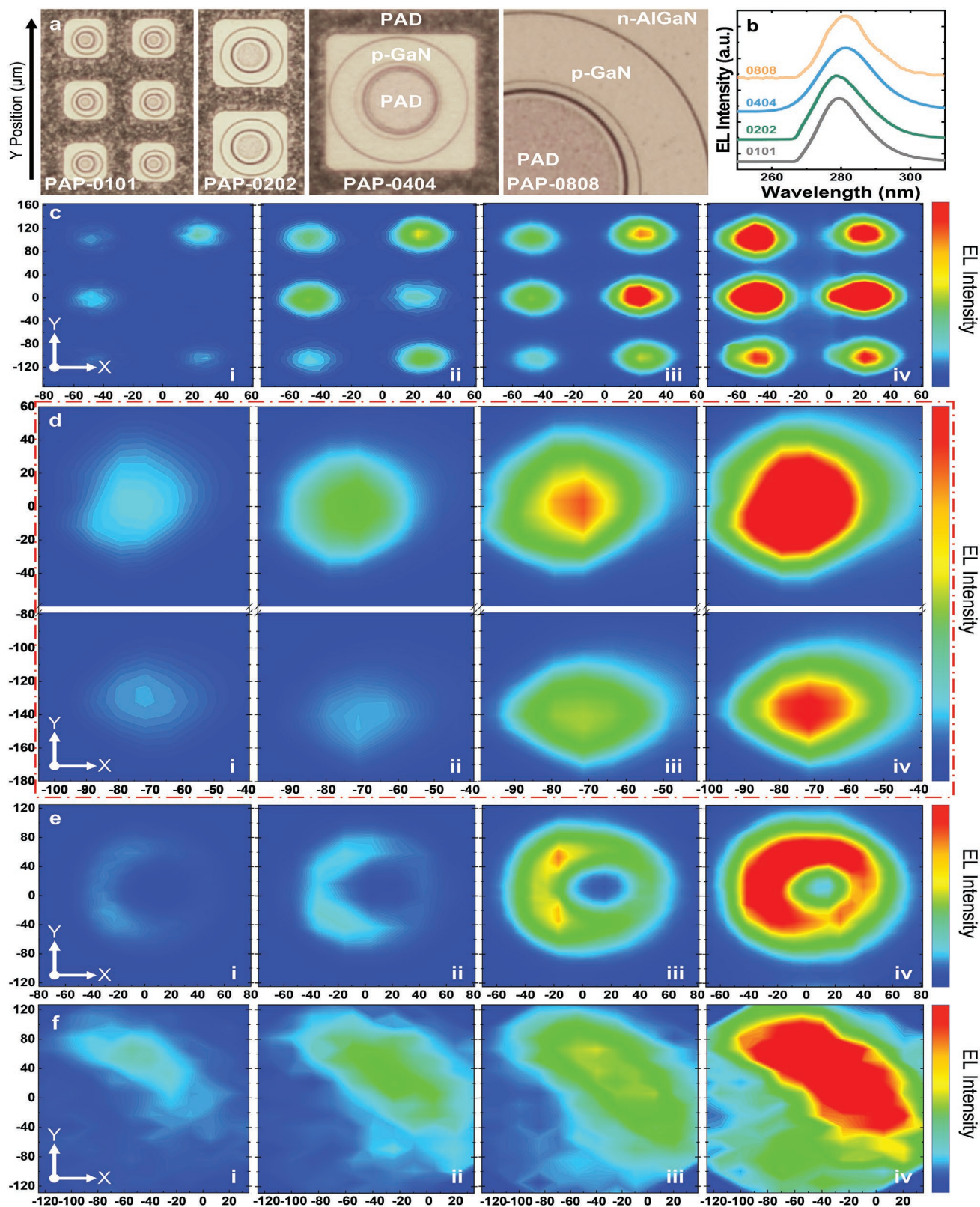
**ADVANCED
SCIENCE NEWS**

www.advancedsciencenews.com

**ADVANCED
MATERIALS**

www.advmat.de

Figure 5. Micro-EL mapping images were recorded with a high-spatial-resolution fluorescence imaging system from 279 to 281 nm. a) Optical microscopy images of PAP-0101, PAP-0202, PAP-0404, and PAP-0808 DUV LEDs. b) EL spectra of PAP-0101, 0202, 0404, and 0808 DUV LEDs under different injection current densities. c–f) The micro-EL mapping images of PAP-0101 under current densities of 161, 174, 187, and 198 A cm^{-2} (c); PAP-0202 under current densities of 198, 221, 243, and 265 A cm^{-2} (d); and PAP-0404 under current densities of 398, 442, 486, and 530 A cm^{-2} (e); and PAP-0808 under current densities of 575, 618, 663, and 707 A cm^{-2} (f).

**ADVANCED
SCIENCE NEWS**

www.advancedsciencenews.com

**ADVANCED
MATERIALS**

www.advmat.de

PAP-0101 and PAP-0202 show considerably enhanced integral emission intensity. Moreover, the emission areas of PAP-0101 and PAP-0202 expand radially from the center to the edge region within each single mesa. On the other hand, PAP-0404 and PAP-0808 have not revealed obvious emission areas expanding from the edge when further increasing the current densities up to 530 and 707 A cm^{-2}, respectively. The emission absence in the central area of PAP-0404 and PAP-0808 is due to the light absorption from p-type electrodes, and insufficient current injection into the central part of the mesa region, which is consistent with the current distribution simulation results, as shown in Figure 2b. In addition, we also investigated the stress distribution of the mesa region by micro-Raman measurements. It is found that the mesa of PAP-0101 has the minimum tensile stress variation between its center and edge region (Figures S4 and S5, Supporting Information). This observation is consistent with the previous reports[22] that suppressing the increment of tensile stress is effective to suppress TM-polarized light. Thus, the LOP of TE-polarized light of PAP-0101 with uniform-distributed emission overall the mesa can be reinforced.

From the above analysis, it should be emphasized that although the simulated LOP values of PAP-0101, PAP-0202, and PAP-0404 are reinforced compared to PAP-0808, and the light absorption loss induced by p-type GaN layer and electrode of PAP-0202 is also improved according to the μ-EL mapping results, the experimental LOP and WPE enhancement factors of PAP-0202 and 0404 are far lower than theoretically predicted values of 20 and 3, respectively. In the simulation section (Figure 1c), only the size and quantity of mesa-dependent LOP of PAP micro-LEDs are considered, which emphasize the contribution of size reduction to the improvement of LOP. How-

ever, in the experiments, two major factors influence the output power and WPE. One is the current crowding effect. As shown in Figure S6 (Supporting Information), the mesas around the edge region of array show a stronger luminescence because most of the injected electrons are crowded in the n-AlGaN layer of this region. The other reason is the heavy self-heating effect that exists in current crowding region, which further degrades the stability and performance of arrayed devices.[28d,e] In order to confirm the self-heating effect, EL spectra of PAP-0101, PAP-0202, PAP-0404, and PAP-0808 are measured at various injected current densities and the results are shown in Figure S7 (Supporting Information). A dependence of the emission wavelength as a function of the current density for four kinds of PAP devices is plotted in Figure S8 (Supporting Information). It can be seen that the redshift of emission wavelength for PAP-0101 is only 1.3 nm when increasing the current density from 350 to 620 A cm^{-2}. However, the values of wavelength redshift are 5.9, 6, and 6.2 nm for PAP-0202, PAP-0404, and PAP-0808, respectively, which are much higher than that of PAP-0101. As a result, the abovementioned two factors co-work interdependently, contributing to the dramatic decrease of LOP and WPE of PAP-0202 compared to PAP-0101.

An excellent Ohmic contact is crucial for improving the device performance, especially for the DUV LEDs where fabricating high-quality p-type contacts, even n-type ones, has always been challenging. In our devices, Ti/Al/Ti/Au (Ni/Au) metal contact layer deposited with electron-beam evaporation was processed by rapid thermal annealing at 950 °C (550 °C) to form the n-type (p-type) Ohmic contact electrode. To evaluate the quality of Ohmic contacts, a circular transmission line model (CTLM) was used to estimate the specific contact resistivity (ρ).[29] The pattern for CTLM is shown in **Figure 6**a, where
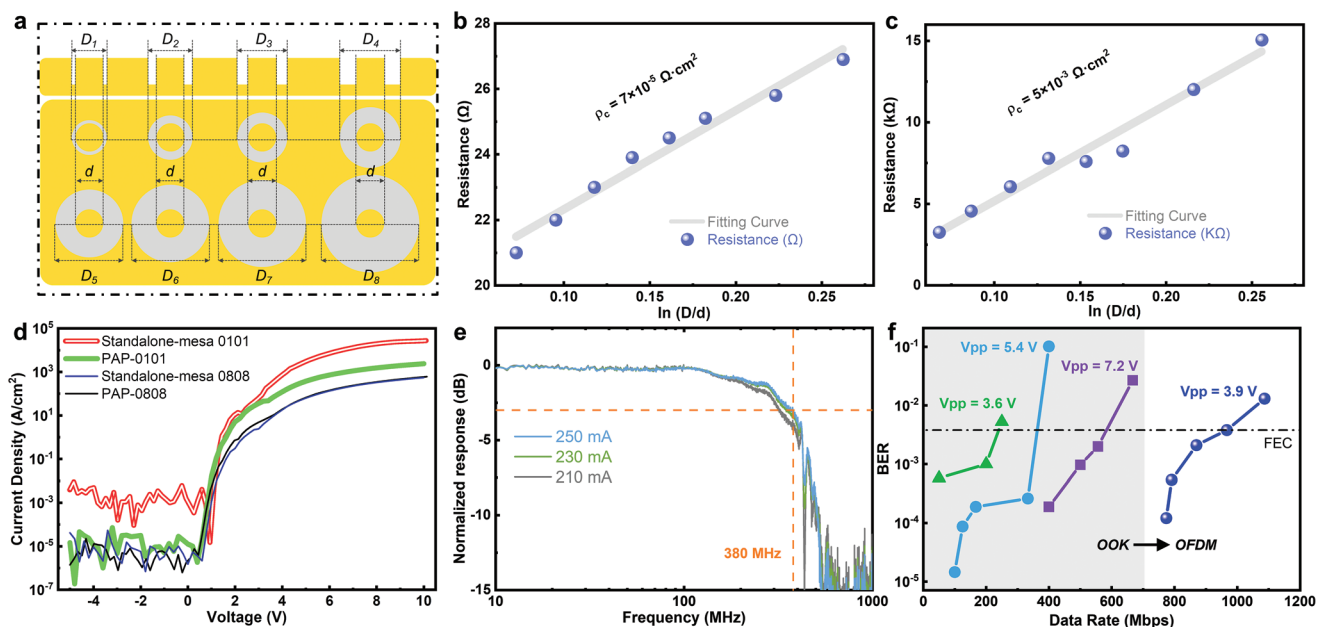

Figure 6. a) Schematic diagram of the circular transmission line model (CTLM). The top panel shows the cross-sectional view of the concentric rings. The bottom panel shows the plan view of the arrayed concentric rings. The orange region and light gray region present the metal electrode and p-type GaN or n-type AlGaN layer, respectively. b,c) The relationship between the $\ln(D/d)$ and measured resistance for n-type (b) and p-type (c) CTLM contacts. d) Current density–voltage characteristic of standalone-mesa 0101/0808 and PAP-0101/PAP-0808. e) Frequency-dependent modulation bandwidth at currents of 210, 230, and 250 mA. f) BER versus data rate at different signal modulation depths.

**ADVANCED
SCIENCE NEWS**

www.advancedsciencenews.com

**ADVANCED
MATERIALS**

www.advmat.de

the circle transmission lines were fabricated with arrayed concentric rings. The inner diameter is designed to be the same and labeled as d, while the different external diameters are labeled as D_i's (i = 1, 2, 3, 4, 5, and 6). The value of ρ can be obtained by fitting the linear relationship between $\ln(D_i/d)$ and the resistance of concentric rings, as shown in Figure 6b,c, which are 7×10^{-5} and 5×10^{-3} Ω cm^2 for n-type and p-type CTLM contacts, respectively. These results exhibit the excellent Ohmic contact quality of our devices.

Based on the above discussions, PAP-0101 is the best candidate for realizing solar-blind light communication, since its high light output power accessed at high current density and small size are promising for applications preferring high modulation bandwidth and long distance.[30a] Afterward, an SBC system was established by PAP-0101, optical lens, and photodiode detectors, which can be seen in Figure S9 (Supporting Information).

As for modulation bandwidth and data rate characterizations, initially, the accessible current density in the linear range of PAP-0101 was measured. As shown in Figure 6d, the current density of PAP-0101 can reach 1000 A cm^{-2} at the bias voltage of 7 V. Although a higher current density over 10^4 A cm^{-2} can be obtained at the same voltage from the standalone-mesa device with a diameter of 25 μm, its LOP is very poor. In addition, the leakage current of PAP-0101 at a bias voltage of −5 V is 10^{-5} A cm^{-2}, which is lower than that of standalone-mesa 0101 due to a larger area of electrodes. It is noted that the current density of standalone micro-LED is about 10^4 A cm^{-2} under a bias voltage of 7 V, while that of PAP-0101 is about 10^3 A cm^{-2}. The smaller current density of the latter one indicates the increased resistance. In consideration of that the encapsulation metal pads, which are also expected to dissipate heating, have the same area, the heating becomes more serious for PAP-0101 with 256 emission mesas. This reduces the mobility of carriers and thus enlarges the device resistance. It is noted in Figure 6d that PAP-0808 and standalone-mesa device 0808 have the similar current density under the same bias voltage, which obviously differs from the case of PAP-0101 because the heating area (emission area) of PAP-0808 is only four times larger than that of standalone-mesa device 0808, much lower than the factor of 256 in PAP-0101. This, in turn, confirms the role of heating played in the resistance increasing of the arrayed device. Then, the frequency-dependent modulation bandwidth was measured at 210, 230, and 250 mA. As shown in Figure 6e, the maximum −3 dB modulation bandwidth of 380 MHz is achieved at 250 mA, which is higher than 285 MHz of 1020 device measured at 50 mA. Unfortunately, the modulation bandwidths of PAP-0202, PAP-0404, and PAP-0808 failed to be detected due to their poor LOP, which were unable to make photodiode detectors get enough response. Details about the frequency-dependent modulation bandwidth characteristics can be seen in Figures S9–S11 (Supporting Information). Finally, an on–off keying (OOK) scheme was used to test the data rate of the PAP-0101. Figure 6f shows the data-rate-dependent bit-error rate (BER) measured with modulation depth varying from 2.7 to 7.2 V at a transmission distance of 0.7 m. Here, the modulation depth describes the AC voltage amplitude that is applied on the LED in its linear range. When the modulation

depth increases to 7.2 V, a maximum data rate of 667 Mbps was achieved at a BER of 2×10^{-2}. A data rate of 557 Mbps was obtained under the forward error correction (FEC) criterion of 2×10^{-3}. The data rate of our work is lower than that of reported values of standalone mesa,[1c] where the data rate of 1.1 Gbps was reported at a distance of 0.3 m by using an orthogonal frequency-division multiplexing (OFDM) scheme. When an OFDM scheme[8b] was performed on PAP-0101 in our measurement, an obvious improvement of the data rate was obtained with the maximum values of 1.087 and 0.97 Gbps at a BER of 1.3×10^{-2} and FEC criterion (BER = 2×10^{-3}), respectively. Most importantly, the transmission distance of PAP-0101 is improved 2.3 times longer than that of previous report.[1c] It is believed that the data rate and transmission distance of PAP micro-LEDs can be further improved by optimizing the device performance, measurement setup configurations, and modulation scheme. Details of the measurements of data rate can be seen in Figure S12 (Supporting Information).

Conventional state-of-the art planar DUV LEDs at 265–280 nm typically show their highest value of WPE at a very small current density (typically lower than 50 A cm^{-2}),[31i] where their LOP value stays at a low level. However, it is desired in many application scenarios that the maximum values of LOP and WPE appear at higher current densities. In contrast, both the LOP and WPE of our PAP micro-LEDs reached their maximum values at a large current density (>700 A cm^{-2}), making them quite preferable for practical applications including sterilization and SBC.

It is noted that, compared with standalone device, several issues related to arrayed micro-LEDs should be emphasized. First, a high uniformity is required for all pixels in the array, to ensure synchronously reaction to electricity signal, which brings about challenges in uniformity for epitaxy growth and the fabrication process. Second, since the arrayed devices are expected to operate at high current densities, their reliability becomes a crucial factor, demanding high crystalline quality for material synthesis and excellent thermal management for device encapsulation.

3. Conclusion

By reducing the diameter of the mesa to 25 μm, an ultra-high power density of over 400 W cm^{-2} was achieved in the standalone-mesa DUV μ-LEDs. Then, by interconnecting 16×16 25 μm diameter mesas to form PAP-0101 DUV μ-LEDs, a remarkable LOP of 83.5 mW at 230 mA was achieved under a current density over 1000 A cm^{-2} by virtue of the suppression of light absorption loss and homogeneous injection current distribution. In addition, the WPE at a large current of 155 mA (775 A cm^{-2}) was as high as 4.7%. Finally, the PAP-0101 DUV μ-LED-based solar-blind communication system has been successfully established with a −3 dB modulation bandwidth of 380 MHz. Our results demonstrate that the high-performance PAP μ-LEDs are an excellent candidate to achieve multifunctional sterilization-co-communication DUV LEDs on chip and are promising to further advocate III-nitride materials for optoelectronic applications.

4. Experimental Section

Theoretical Simulation: Monte Carlo ray-tracing simulation and current distribution simulation were implemented by the finite element method. The absorption coefficients of AlGaN and GaN at the wavelength of 279 nm in ray-tracing simulation were set as 10 and 19 900 cm^{-1}, respectively.[32] The refractive indices of sapphire, GaN, AlN, and SiO$_2$ are 1.75, 2.59, 2.31, and 1.50, respectively.[32b,33] The refractive index of Al$_x$Ga$_{1-x}$N has a relationship with its bandgap E_g (hv)

as $n(hv) = \left\{ a \left(\dfrac{hv}{E_g} \right)^{-2} \left[2 - \left(1 + \dfrac{hv}{E_g} \right)^{0.5} - \left(1 - \dfrac{hv}{E_g} \right)^{0.5} \right] + b \right\}^{0.5}$, where h and

v are the Planck constant and light frequency, respectively, and a and b are fitting parameters varying with molar fraction x.[33a,34]

MOCVD Growth of DUV LED Wafers: The DUV LED wafer was grown on sapphire substrate by MOCVD, comprising an AlN buffer layer, a 3 μm-thick AlN layer, a 1.5 μm-thick n-type A$_{0.64}$Ga$_{0.36}$N layer, five periods of Al$_{0.5}$Ga$_{0.5}$N/Al$_{0.42}$Ga$_{0.58}$N multiple quantum wells, a 10 nm-thick high-Al-composition AlGaN electron-blocking layer, 40 nm-thick p-type AlGaN layer, and a 10 nm-thick p-type heavily doped GaN contact layer.

LED Fabrication Process: The standard semiconductor process was used to fabricate LED devices in this work, including stepper photolithography, inductively coupled plasma reactive ion etching (ICP-RIE), plasma-enhanced chemical vapor deposition (PECVD), electron-beam evaporation, rapid thermal annealing, and laser cutting and dicing.

Characterization: The transient PL spectra were measured by PicoQuant's time-resolved photoluminescence (TRPL) spectroscopy. Raman spectra and EL mapping for DUV PAP micro-LEDs were measured by HORIBA's photoluminescence and electroluminescence system.

Bandwidth and Data Rate Measurements: First, AC frequency sweep signals generated by a vector network analyzer (Pico VNA 106) were coupled to a direct current (DC) signal via a bias-tee (Mini-circuit ZFBT-6GW+, 0.1–6000 MHz). Then, the coupled electrical signal was loaded into the PAP-0101 μ-LED whose light signals were collected by a high-sensitivity avalanche photodiode (APD, Thorlabs APD430A2/M, 400 MHz, 14 A W^{-1}). Finally, the amplitude–frequency characteristics were analyzed by the vector network analyzer to estimate the modulation bandwidth. As for the data rate measurement, a free-space optical communication system was established with a PAP-0101 μ-LED being a transmitter. The on–off keying (OOK) modulation signal generated by a signal quality analyzer (Anritsu, MP1800) was coupled with the DC voltage (Keithley 2614B) through the bias-tee (ZFBT-6GW+), before being loaded into PAP-0101 μ-LED by a high-speed probe (Cascade Microtech ACP40-A-GS-400). Finally, the light signal was detected by an APD and transferred to the signal quality analyzer (Anritsu, MP1800) to characterize the relationship between BER and data rate. The orthogonal frequency division multiplexing (16-QAM-OFDM) data generated by an offline MATLAB program were first uploaded to the arbitrary waveform generator (AWG, Tektronix AWG710B, 4.2 Gsa s^{-1}). The AWG converted the digital signal to output electrical signal whose peak-to-peak voltage was then amplified by an amplifier (Mini-circuit ZX60-43-S+). Afterward, the signal was coupled with the DC voltage (Keithley 2614B) which was used to drive the PAP-0101 μ-LED through the bias-tee (ZFBT-6GW+). Finally, the light signal was detected by an APD, and the corresponding electrical signal was captured by an oscilloscope (OSC, Agilent DSA90604A Infiniium, 20 Gsa s^{-1}). The received signal was downloaded to the offline MATLAB program for further analysis.

Supporting Information

Supporting Information is available from the Wiley Online Library or from the author.

Conflict of Interest

The authors declare no conflict of interest.

Data Availability Statement

The data that support the findings of this study are available on request from the corresponding author. The data are not publicly available due to privacy or ethical restrictions.

[1] a) M. Z. Baten, S. Alam, B. Sikder, A. Aziz, *Photonics* **2021**, *8*, 430; b) J. Han, M. H. Crawford, R. J. Shul, J. J. Figiel, M. Banas, L. Zhang, Y. K. Song, H. Zhou, A. V. Nurmikko, *Appl. Phys. Lett.* **1998**, *73*, 1688; c) X. Y. He, E. Y. Xie, M. S. Islm, A. A. Purwita, J. J. D. Mckendry, E. D. Gu, H. Haas, M. D. Dawson, *Photonics Res.* **2019**, *7*, B41.

[2] Z. Xu, B. M. Sadler, *IEEE Commun. Mag.* **2008**, *46*, 67.

[3] D. Moriarty, B. Hombs in *MILCOM 2009 - 2009 IEEE Military Communications Conf.*, IEEE, Boston, Massachusetts, USA **2009**, https://doi.org/10.1109/MILCOM.2009.5379755.

[4] D. E. Sunstein, *Ph.D. Dissertation*, Massachusetts Institute of Technology, Cambridge, MA, USA **1968**.

[5] a) H. M. Kim, T. W. Kang, K. S. Chung, *Adv. Mater.* **2003**, *15*, 567; b) T. H. Lee, T. H. Park, H. W. Shin, N. Maeda, M. Jo, H. Hirayama, B.-H. Kim, T. G. Kim, *Adv. Opt. Mater.* **2020**, *8*, 1901430; c) Z. Chen, Z. Liu, T. Wei, S. Yang, Z. Dou, Y. Wang, H. Ci, H. Chang, Y. Qi, J. Yan, J. Wang, Y. Zhang, P. Gao, J. Li, Z. Liu, *Adv. Mater.* **2019**, *31*, 1807345; d) J. Yu, L. Wang, Z. Hao, Y. Luo, C. Sun, J. Wang, Y. Han, B. Xiong, H. Li, *Adv. Mater.* **2020**, *32*, 1903407; e) M. Tian, H. Yu, M. H. Memon, Z. Xing, C. Huang, H. Jia, H. Zhang, D. Wang, S. Fang, H. Sun, *Opt. Lett.* **2021**, *46*, 4809; f) H. Yu, M. H. Memon, D. Wang, Z. Ren, H. Zhang, C. Huang, M. Tian, H. Sun, S. Long, *Opt. Lett.* **2021**, *46*, 3271; g) H. Ci, H. Chang, R. Wang, T. Wei, Y. Wang, Z. Chen, Y. Sun, Z. Dou, Z. Liu, J. Li, P. Gao, Z. Liu, *Adv. Mater.* **2019**, *31*, 1970211; h) Z. Zhong, X. Zheng, J. Li, J. Zheng, Y. Zang, W. Lin, J. Kang, *Phys. Status Solidi A* **2019**, *216*, 1900059; i) H. Sun, M. K. Shakfa, M. M. Muhammed, B. Janjua, K.-H. Li, R. Lin, T. K. Ng, I. S. Roqan, B. S. Ooi, X. Li, *ACS Photonics* **2018**, *5*, 964; j) D. Li, K. Jiang, X. Sun, C. Guo, *Adv. Opt. Photonics* **2018**, *10*, 43; k) Y. Chen, J. Ben, F. Xu, J. Li, Y. Chen, X. Sun, D. Li, *Fundam. Res.* **2021**, *1*, 717; l) T. Wei, S. Islam, U. Jahn, J. Yan, K. Lee,

S. Bharadwaj, X. Ji, J. Wang, J. Li, V. Protasenko, *Opt. Lett.* **2020**, *45*, 121; m) T.-C. Hsu, Y.-T. Teng, Y.-W. Yeh, X. Fan, K.-H. Chu, S.-H. Lin, K.-K. Yeh, P.-T. Lee, Y. Lin, Z. Chen, T. Wu, H.-C. Kuo, *Photonics* **2021**, *8*, 196; n) S.-H. Lin, M.-C. Tseng, K.-W. Peng, S. Lai, M.-C. Shen, R.-H. Horng, S.-Y. Lien, D.-S. Wuu, H.-C. Kuo, T. Wu, Z. Chen, *Opt. Express* **2021**, *29*, 37835.

[6] a) K. A. Sholtes, K. Lowe, G. W. Walters, M. D. Sobsey, K. G. Linden, L. M. Casanova, *Environ. Technol.* **2016**, *37*, 2183; b) J. F. Ready, *Industrial Applications of Lasers*, Elsevier, Amsterdam, The Netherlands **1997**; c) W. Van Bommel, *Road Lighting: Fundamentals, Technology and Application*, Springer, Berlin, Germany **2014**.

[7] a) Z. Gong, S. Jin, Y. Chen, J. McKendry, D. Massoubre, I. M. Watson, E. Gu, M. D. Dawson, *J. Appl. Phys.* **2010**, *107*, 013103; b) J. J. D. McKendry, D. Massoubre, S. Zhang, B. R. Rae, R. P. Green, E. Gu, R. K. Henderson, A. E. Kelly, M. D. Dawson, *J. Lightwave Technol.* **2012**, *30*, 61; c) R. P. Green, J. J. D. McKendry, D. Massoubre, E. Gu, M. D. Dawson, A. E. Kelly, *Appl. Phys. Lett.* **2013**, *102*, 091103; d) W. Yang, S. Zhang, J. J. D. McKendry, J. Herrnsdorf, P. Tian, Z. Gong, Q. Ji, I. M. Watson, E. Gu, M. D. Dawson, L. Feng, C. Wang, X. Hu, *J. Appl. Phys.* **2014**, *116*, 044512; e) R. McClintock, A. Haddadi, M. Razeghi, *Proc. SPIE* **2012**, *8268*, 826810.

[8] a) O. Alkhazragi, F. Hu, P. Zou, Y. Ha, C. H. Kang, Y. Mao, T. K. Ng, N. Chi, B. S. Ooi, *Opt. Express* **2020**, *28*, 9111; b) S. Zhu, P. Qiu, Z. Qian, X. Shan, Z. Wang, K. Jiang, X. Sun, X. Cui, G. Zhang, D. Li, P. Tian, *Opt. Lett.* **2021**, *46*, 2147.

[9] H. Kawanishi, M. Senuma, T. Nukui, *Proc. SPIE* **2007**, *6473*, 64731D.

[10] P. Manley, S. Walde, S. Hagedorn, M. Hammerschmidt, S. Burger, C. Becker, *Opt. Express* **2020**, *28*, 3619.

[11] a) H.-D. Kim, H.-M. An, K. H. Kim, S. J. Kim, C. S. Kim, J. Cho, E. F. Schubert, T. G. Kim, *Adv. Funct. Mater.* **2014**, *24*, 1575; b) Z. Huang, Z. Zhong, H. Wang, S. Lu, J. Wang, G. Liu, T. Wei, J. Yan, J.-H. Min, W. L. Jeong, D.-S. Lee, X. Cai, F. Xu, X. Chen, D. Cai, J. Wang, J. Kang, *J. Phys. Chem. Lett.* **2020**, *11*, 2559.

[12] a) D. Y. Kim, J. H. Park, J. W. Lee, S. Hwang, S. J. Oh, J. Kim, C. Sone, E. F. Schubert, J. K. Kim, *Light: Sci. Appl.* **2015**, *4*, e263; b) T. Takano, T. Mino, J. Sakai, N. Noguchi, K. Tsubaki, H. Hirayama, *Appl. Phys. Express* **2017**, *10*, 031002; c) X. Peng, W. Guo, H. Xu, L. Chen, Z. Yang, L. Xu, K. Tang, C. Guo, L. Yan, S. Guo, C. Chen, J. Ye, *Appl. Phys. Express* **2021**, *14*, 072005.

[13] N. Lobo, H. Rodriguez, A. Knauer, M. Hoppe, S. Einfeldt, P. Vogt, M. Weyers, M. Kneissl, *Appl. Phys. Lett.* **2010**, *96*, 081109.

[14] C. Pernot, M. Kim, S. Fukahori, T. Inazu, T. Fujita, Y. Nagasawa, A. Hirano, M. Ippommatsu, M. Iwaya, S. Kamiyama, I. Akasaki, H. Amano, *Appl. Phys. Express* **2010**, *3*, 061004.

[15] P. Dong, J. Yan, J. Wang, Y. Zhang, C. Geng, T. Wei, P. Cong, Y. Zhang, J. Zeng, Y. Tian, L. Sun, Q. Yan, J. Li, S. Fan, Z. Qin, *Appl. Phys. Lett.* **2013**, *102*, 241113.

[16] G.-D. Hao, M. Taniguchi, N. Tamari, S.-I. Inoue, *J. Phys. D: Appl. Phys.* **2017**, *51*, 035103.

[17] I. Eliashevich, Y. Li, A. Osinsky, C. A. Tran, M. G. Brown, R. F. Karlicek Jr., *Proc. SPIE* **1999**, *3621*, 28.

[18] a) T.-M. Chen, S.-J. Wang, K.-M. Uang, S.-L. Chen, W.-C. Tsai, W.-C. Lee, C.-C. Tsai, *Appl. Phys. Lett.* **2007**, *90*, 041115; b) W. Shui-Jinn, C. Shiue-Lung, U. Kai-Ming, L. Wei-Chi, C. Tron-Min, C. Chao-Hsuing, L. Bor-wen, *IEEE Photonics Technol. Lett.* **2006**, *18*, 1146.

[19] a) M. Shatalov, G. Simin, V. Adivarahan, A. Chitnis, S. Wu, R. Pachipulusu, V. Mandavilli, K. Simin, J. P. Zhang, J. W. Yang, *Jpn. J. Appl. Phys.* **2002**, *41*, 5083; b) V. Adivarahan, S. Wu, W. Sun, V. Mandavilli, M. Shatalov, G. Simin, J. Yang, H. Maruska, M. A. Khan, *Appl. Phys. Lett.* **2004**, *85*, 1838.

[20] J. K. Kim, J.-Q. Xi, H. Luo, E. F. Schubert, J. Cho, C. Sone, Y. Park, *Appl. Phys. Lett.* **2006**, *89*, 141123;

[21] J. W. Lee, J. H. Park, D. Y. Kim, E. F. Schubert, J. Kim, J. Lee, Y.-I. Kim, Y. Park, J. K. Kim, *ACS Photonics* **2016**, *3*, 2030.

[22] J. Zheng, J. Li, Z. Zhong, W. Lin, L. Chen, K. Li, X. Wang, C. Chou, S. Li, J. Kang, *RSC Adv.* **2017**, *7*, 55157.

[23] M. L. Nakarmi, K. H. Kim, K. Zhu, J. Y. Lin, H. X. Jiang, *Appl. Phys. Lett.* **2004**, *85*, 3769.

[24] S. Tu, J. Chen, F. Hwu, G. Sheu, F. Lin, S. Kuo, J. Chang, C. Lee, *Solid-State Electron.* **2010**, *54*, 1438.

[25] V. K. Malyutenko, S. S. Bolgov, A. D. Podoltsev, *Appl. Phys. Lett.* **2010**, *97*, 251110.

[26] S. Liu, W. Luo, D. Li, Y. Yuan, W. Tong, J. Kang, Y. Wang, D. Li, X. Rong, T. Wang, Z. Chen, Y. Li, H. Wang, W. Wang, J. Hoo, L. Yan, S. Guo, B. Shen, Z. Cong, X. Wang, *Adv. Funct. Mater.* **2020**, *31*, 2008452.

[27] R. Floyd, M. Gaevski, M. D. Alam, S. Islam, K. Hussain, A. Mamun, S. Mollah, G. Simin, M. V. S. Chandrashekhar, A. Khan, *Appl. Phys. Express* **2021**, *14*, 014002.

[28] a) J. M. Smith, R. Ley, M. S. Wong, Y. H. Baek, J. H. Kang, C. H. Kim, M. J. Gordon, S. Nakamura, J. S. Speck, S. P. DenBaars, *Appl. Phys. Lett.* **2020**, *116*, 071102; b) J. Zhan, Z. Chen, Q. Jiao, Y. Feng, C. Li, Y. Chen, Y. Chen, F. Jiao, X. Kang, S. Li, Q. Wang, T. Yu, G. Zhang, B. Shen, *Opt. Express* **2018**, *26*, 5265; c) S. Chichibu, T. Azuhata, T. Sota, S. Nakamura, *Appl. Phys. Lett.* **1996**, *69*, 4188; d) A. Chitnis, J. Sun, V. Mandavilli, R. Pachipulusu, S. Wu, M. Gaevski, V. Adivarahan, J. P. Zhang, M. A. Khan, A. Sarua, M. Kuball, *Appl. Phys. Lett.* **2002**, *81*, 3491; e) B. Yan, D. Teng, L. Liu, G. Wang, in *2018 19th Int. Conf. on Electronic Packaging Technology (ICEPT)*, IEEE, Piscataway, NJ, USA **2018**, pp. 168–175.

[29] a) G. Reeves, *Solid-State Electron.* **1980**, *23*, 487.

[30] a) S. Zhu, S. Lin, J. Li, Z. Yu, H. Cao, C. Yang, J. Li, L. Zhao, *Appl. Phys. Lett.* **2017**, *111*, 171105; b) A. Rashidi, M. Monavarian, A. Aragon, A. Rishinaramangalam, D. Feezell, *IEEE Electron Device Lett.* **2018**, *39*, 520.

[31] a) M. Shatalov, W. Sun, A. Lunev, X. Hu, A. Dobrinsky, Y. Bilenko, J. Yang, M. Shur, R. Gaska, C. Moe, G. Garrett, M. Wraback, *Appl. Phys. Express* **2012**, *5*, 082101; b) J. R. Grandusky, J. Chen, S. R. Gibb, M. C. Mendrick, C. G. Moe, L. Rodak, G. A. Garrett, M. Wraback, L. J. Schowalter, *Appl. Phys. Express* **2013**, *6*, 032101; c) M. Kneissl, T.-Y. Seong, J. Han, H. Amano, *Nat. Photonics* **2019**, *13*, 233; d) H. Hirayama, S. Fujikawa, N. Noguchi, J. Norimatsu, T. Takano, K. Tsubaki, N. Kamata, *Phys. Status Solidi A* **2009**, *206*, 1176; e) H. Hirayama, Y. Tsukada, T. Maeda, N. Kamata, *Appl. Phys. Express* **2010**, *3*, 031002; f) R.-H. Hrong, Y.-Y. Zeng, W.-K. Wang, C.-L. Tsai, Y.-K. Fu, W.-H. Kuo, *Opt. Express* **2017**, *25*, 32206; g) A. Fujioka, T. Misaki, T. Murayama, Y. Narukawa, T. Mukai, *Appl. Phys. Express* **2010**, *3*, 041001; h) S.-i. Inoue, N. Tamari, M. Taniguchi, *Appl. Phys. Lett.* **2017**, *110*, 141106; i) C. J. Zollner, A. S. Almogbel, Y. Yao, M. Wang, M. Iza, J. S. Speck, S. P. DenBaars, S. Nakamura, *Opt. Mater. Express* **2020**, *10*, 2171.

[32] a) T. Kawashima, H. Yoshikawa, S. Adachi, S. Fuke, K. Ohtsuka, *J. Appl. Phys.* **1997**, *82*, 3528; b) J. F. Muth, J. D. Brown, M. A. L. Johnson, Z. Yu, R. M. Kolbas, J. W. Cook, J. F. Schetzina, *MRS Internet J. Nitride Semicond. Res.* **1999**, *4*, 502.

[33] a) G. M. Laws, E. C. Larkins, I. Harrison, C. Molloy, D. Somerford, *J. Appl. Phys.* **2001**, *89*, 1108; b) M. Querry, Optical Constants, US Army Chemical Research, Development and Engineering Center (CRDC), Aberdeen Proving Ground, Aberdeen, MD, USA **1985**, p. 418; https://ui.adsabs.harvard.edu/abs/1985umo..rept.....Q; c) L. V. Rodríguez-de Marcos, J. I. Larruquert, J. A. Méndez, J. A. Aznárez, *Opt. Mater. Express* **2016**, *6*, 3622.

[34] T. Peng, J. Piprek, *Electron. Lett.* **1996**, *32*, 2285.